electronics

MDPI

Article

High-Power Electromagnetic Pulse Effect Prediction for Vehicles Based on Convolutional Neural Network

Le Cao [1,2,*], Shuai Hao [1], Yuan Zhao [3] and Cheng Wang [4]

[1] School of Electric and Control Engineering, Xi'an University of Science and Technology, Xi'an 710054, China; haoxust@xust.edu.cn
[2] School of Electrical Engineering, Xi'an Jiaotong University, Xi'an 710049, China
[3] School of Electronic Engineering, Chengdu University of Information Technology, Chengdu 610225, China; zhaoyuan@cuit.edu.cn
[4] Qian Xuesen Laboratory of Space Technology, China Academy of Space Technology, Beijing 100094, China; wangcheng@qxslab.cn
* Correspondence: caole@xust.edu.cn

Abstract: This study presents a prediction model for high-power electromagnetic pulse (HPEMP) effects on aboveground vehicles based on convolutional neural networks (CNNs). Since a vehicle is often located aboveground and is close to the air-ground_half-space interface, the electromagnetic energy coupled into the vehicle by the ground reflected waves cannot be ignored. Consequently, the analysis of the vehicle's HPEMP effect is a composite electromagnetic scattering problem of the half-space and the vehicles above it, which is often analyzed using different half-space numerical methods. However, traditional numerical methods are often limited by the complexity of the actual half-space models and the high computational demands of complex targets. In this study, a prediction method is proposed based on a CNN, which can analyze the electric field and energy density under different incident conditions and half-space environments. Compared with the half-space finite-difference time-domain (FDTD) method, the accuracy of the prediction results was above 98% after completing the training of the CNN network, which proves the correctness and effectiveness of the method. In summary, the CNN prediction model in this study can provide a reference for evaluating the HPEMP effect on the target over a complex half-space medium.

Keywords: vehicle electromagnetic coupling; high-power electromagnetic pulse; half-space; deep learning; convolutional neural network

Citation: Cao, L.; Hao, S.; Zhao, Y.; Wang, C. High-Power Electromagnetic Pulse Effect Prediction for Vehicles Based on Convolutional Neural Network. *Electronics* **2022**, *11*, 1490. https://doi.org/10.3390/electronics11091490

Academic Editors: Mingyao Xia and Dazhi Ding

Received: 7 April 2022
Accepted: 5 May 2022
Published: 6 May 2022

1. Introduction

With the rapid development of high-power electromagnetic pulse (HPEMP) technologies and the widespread application of electronic systems and equipment in vehicles, the electromagnetic environment of vehicles is extremely complex. Consequently, the study of HPEMP coupling effects in sensitive electronic systems is of great importance [1,2]. It is noted that HPEMPs have a strong energy and wide frequency spectrum, which not only can cause direct disability to the electronic systems of vehicles but also can interfere with or damage the electronic control system by powerful coupling through windows, apertures, or antennas [3–5]. Therefore, studying the coupling effect on vehicles under HPEMP can provide a reference for vehicular electromagnetic pulse protection technology and lay a theoretical foundation for improving the vehicle's anti-electromagnetic interference ability.

From the perspective of computational electromagnetism, the HPEMP effect on vehicles is a composite time-domain scattering problem. Numerous numerical approaches have been widely used, such as the Method of Moments (MoM) [6,7], the Finite-Difference Time-Domain (FDTD) method [8–10], the Finite Element Method (FEM) [11,12], the Time-Domain Integral Equation (TDIE) method [13,14], and other hybrid methods [15,16]. However, to calculate the coupling between the vehicle and the half-space, most existing algorithms

need to use half-space Green's function, which is extremely difficult to derive and calculate, particularly for multi-layered planar medium and rough surfaces. In addition, the HPEMP effect is exceedingly sensitive to initial conditions; however, numerical methods require remodeling and calculation for different initial conditions, which have a high demand on computational memory and time. Therefore, the application of existing numerical methods is often limited by computing resources and half-space Green's function, which makes it difficult to meet the demands of the vehicle's HPEMP effect analysis.

In addition, the coupling fields within a vehicle are very sensitive to the initial conditions, such as incident conditions, the location of the observation point, the incoming frequency, etc. Small changes in these parameters can result in a significantly different coupling field distribution within a vehicle. Once the initial conditions are changed, the numerical method needs to be remodeled and calculated, which consumes a lot of computational resources. Consequently, numerical methods may not be efficient enough in an HPEMP analysis. To address the above problems, we designed a concise and effective framework using the half-space FDTD method and deep learning. Convolutional neural networks (CNNs) have demonstrated attractive capabilities for both regression and categorization applications. They have been applied in various electromagnetic engineering problems, including rough surface parameter inversions [17], inverse scattering problems [18], shielding effectiveness calculations [19], and radar target recognition and classification [20,21]. In this study, an HPEMP effect analysis method based on a CNN is proposed, which can be applied to predict the characteristics of the electric field of the observation point inside a vehicle above half-space. Compared with existing methods, this study makes the following main contributions:

(1) The HPEMP effect prediction based on LeNet-5, VGG-16, and GoogleNet was introduced. The experiments show that the proposed method significantly improves the efficiency and performance of predictions.
(2) The ground reflected wave was used instead of the half-space Green's function to analyze the HPEMP effect on the lower half-space of the vehicle; therefore, it can be used for the prediction of HPEMP effects under various half-space environments.
(3) The possibility of using CNN for computational electromagnetics in electromagnetic interference (EMI) analyses was discussed.

The rest of this paper is organized as follows. Section 2 introduces the methodologies, including the half-space FDTD method and the proposed CNN model. In Section 3, the correctness and effectiveness of the proposed method are verified. The coupling of the electric field was then predicted and analyzed. Finally, conclusions are made in Section 4.

2. Methodology

2.1. Datasets Generated by Half-Space FDTD

A schematic diagram of the half-space scattering problem is presented in Figure 1. In this case, the total incident wave of the target includes two parts: the direct incident wave and the reflected wave of the half-space interface. The incident plane was defined as the plane created by the k-and z-axes. Assume that α_0 represents the incident wave's polarization angle. The incident wave's electric field can be split into two components: a horizontal component (perpendicular to the incident plane) and a vertical component.

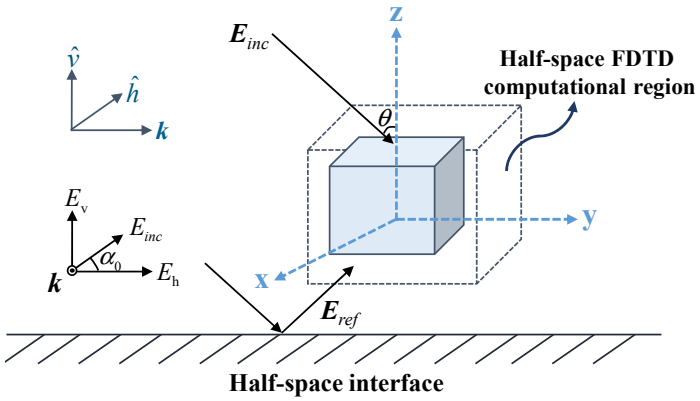

Figure 1. Scattering problem of the target over half-space.

Generally, the reflected wave is dependent on both the magnitude of the electric field and its polarization state. When an incident wave is linearly polarized, the reflected wave is typically elliptically polarized. The polarization angle α and ellipticity angle β of the reflected wave can be written as follows:

$$\alpha = \frac{1}{2}\tan^{-1}\left(\frac{2e_{rh}e_{rv}\cos\psi_r}{e_{rh}^2 - e_{rv}^2}\right) \beta = \frac{1}{2}\sin^{-1}\left(\frac{2e_{rh}e_{rv}\sin\psi_r}{e_{rh}^2 + e_{rv}^2}\right), \tag{1}$$

where ψ_r denotes the phase difference between the reflected wave's horizontal and vertical components, and

$$e_{rh} = \left|R^{TM}\right|E_0\cos\alpha_0\ e_{rv} = \left|R^{TE}\right|E_0\sin\alpha_0, \tag{2}$$

where R^{TE} and R^{TM} are the TE and TM wave reflection coefficients, which are related to the incident angle and the half-space parameters, respectively. The enhanced half-space FDTD approach [18] was applied in this work to determine the observation point's time-domain response. By setting two 1-D FDTD iterative expressions, the total incident wave can be integrated into the total-field region during FDTD computation. A 3-D FDTD iteration can then be used to obtain the electric field at the observation point.

The simulation model of the vehicle cab used in this study is shown in Figure 2. The vehicle cab has three windows, that is, W1, W2, and W3, in which the media parameters are set as $\varepsilon_r = 4.82, \sigma = 0S \cdot \mathrm{m}^{-1}$. Except for these three windows, the rest of the cab is made of Perfect Electric Conducting (PEC). Since a high-altitude nuclear electromagnetic pulse (HEMP) covers the intermediate frequency (MF), the high frequency (HF), the very high frequency (VHF), and some ultra-high frequency (UHF) bands, it has the characteristics of a wide radiation range, a high intensity, and a wide spectrum. Consequently, the HEMP is set as the incident wave, which can be expressed as follows:

$$E = kE_0\left[\exp\left(-at'\right) - \exp\left(-bt'\right)\right]. \tag{3}$$

In the above formula, $E_0 = 50\mathrm{kV/m}$, $k = 1.05$, $a = 4.0 \times 10^{-6}\mathrm{s}$, and $b = 4.76 \times 10^{-8}\mathrm{s}$, where E_0 is the peak field strength, k is the correction coefficient, and a and b are pulse parameters. $\delta = 8 \times 10^{-3}$ m, and $\Delta t = 0.00625$ ns is the discrete grid and time step size used in the half-space FDTD calculation. In the FDTD calculation, the CPML absorbing boundary is employed.

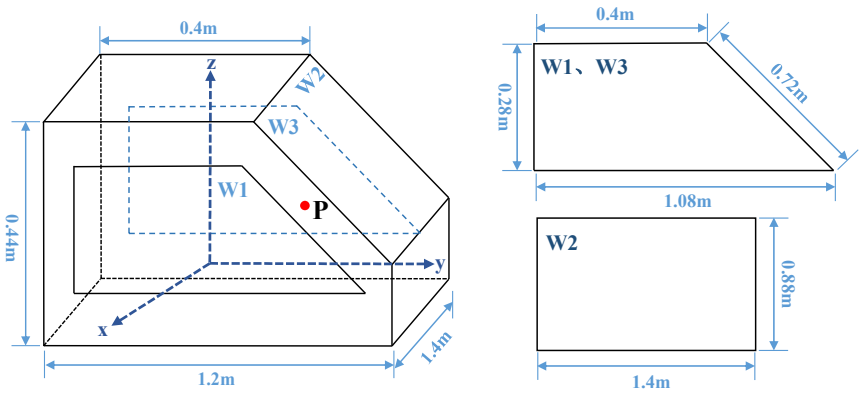

Figure 2. Geometry of 3-D vehicle cab.

The electronic control unit (ECU), which contains various types of chips and electronic devices, is the core component of the vehicle engine's electronic control system. Hence, the ECU is an important and sensitive part of the high-power electromagnetic pulse coupling interference system. Thus, in order to observe the electric field distribution near the ECU, the observation point P (0 m, 0.08 m, 0.096 m) is set. To train the CNN, five essential parameters of the vehicles over half-space are set as the input data, including incident wave parameters (incident angles θ_i and φ_i, polarization angle α_0) and half-space medium parameters (relative permittivity ε_r and electrical conductivity σ). The value ranges of the above parameters are listed in Table 1. The electric field value $E(t)$ of the ECU inside the vehicle is used as the output data. The input parameters can be discretized as follows:

$$A = [\theta_{in}, \varphi_{in}, \alpha_{0n}, \varepsilon_{rn}, \sigma_n], \tag{4}$$

where $n = 1, 2, \ldots, N$, and N is the number of samples in the training set. The value ranges of the input data are listed in Table 1. In this study, the half-space FDTD method was used to calculate the electric field value of the ECU for different incident angles, polarization angles, and half-space medium parameters. A total of 1080 sets of data were obtained. To train the CNN, 80% of the dataset was randomly selected as the training set, and the remaining 20% was selected as the testing set to cross-validate the performance of the established networks.

Table 1. Value range of input data.

Parameters	Description	Range
θ	Incident angle	$0^\circ \sim 90^\circ$
φ	Incident azimuth angle	$0^\circ \sim 180^\circ$
α	Polarization angle	$0^\circ \sim 90^\circ$
ε_r	Dielectric constant of half-space	$1 \sim 10$
σ	Conductivity of half-space	$0 \sim 50 (S \cdot \mathrm{m}^{-1})$

2.2. Network Architecture and Training

Convolutional neural networks have been used to solve many different artificial intelligence problems, providing significant advantages in solving nonlinear, multiparameter learning tasks, such as HPEMP effects. A flowchart of the proposed method is presented in Figure 3. First, the half-space FDTD method was used to calculate the electric field distribution inside the vehicle under the HPEMP and generate data samples of the different incident angles, polarization angles, and half-space parameters. The simulated results were then used to train a CNN to predict the electric field distribution inside vehicles. In addition, a comparison between the prediction results and the numerical method results is provided. The technical details of each step are described below.

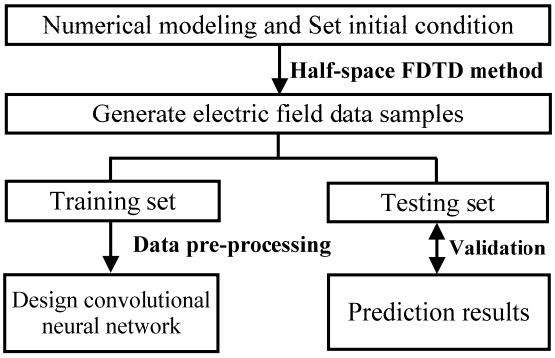

Figure 3. Overall framework of the proposed CNN model.

The basic structure of a CNN mainly includes an input, a convolutional layer, a pooling layer, and fully connected and output layers, in which the convolutional and the pooling layers usually have multiple layers according to practical problems. As shown in Figure 4, the established CNN consists of convolutional layers C1, C3, and C5, pooling layers S2 and S4, and one fully connected layer F6, which are all followed by a rectified linear unit with nonlinearity [22]. The final fully connected layer feeds into a Euclidean loss layer for regression. To reduce overfitting, a dropout layer is applied [23]. In this study, we use the coefficient of determination R^2 to optimize the loss between the true values and model predictions. R^2 is expressed as follows:

$$R^2 = 1 - \frac{\sum_{i=1}^{N}(y_i - \hat{y}_i)^2}{\sum_{i=1}^{N}(y_i - \overline{y}_i)^2}, \tag{5}$$

where y_i, $\overline{y}_i$, and $\hat{y}$ are the actual value, the mean of the actual values, and the predicted value, respectively. N is the number of predicted results. The closer the value of R^2 is to 1, the higher the prediction accuracy and the better the generalization ability of the CNN.

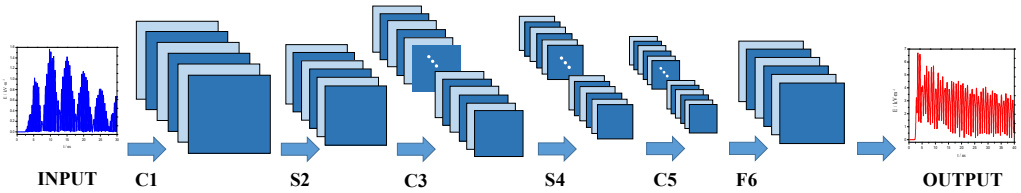

Figure 4. CNN structure of proposed method.

3. Numerical Experiments and Analysis

3.1. Numerical Validation

The performance of the proposed approach was evaluated by comparing the difference in accuracy between the results of the traditional half-space FDTD with those predicted by the CNN regression model. The observation point P (0 m, 0.08 m, and 0.096 m) is set at the position of the ECU, and the incident wave is a HEMP pulse. Thus, the input data is set as $A = (\theta_i, \varphi_i, \alpha_0, \varepsilon_r, \sigma)$, where $\theta_i, \varphi_i, \alpha_0$ are the incident wave parameters, and ε_r, σ are the half-space medium parameters. A comparison between the proposed CNN and the traditional half-space FDTD methods of analyzing the electric field at the observation point P is given in Figure 5. The incident parameters are set as $A = (60°, 90°, 45°, 4, 0.1S/\mathrm{m})$. Figure 6 shows the two-dimensional electric field distribution of the vehicle model at different time steps. From Figure 6 we can see the distribution of the electric field in any observation plane at different time steps, so as to observe the change process of the electric field after the incident wave is coupled into the target.

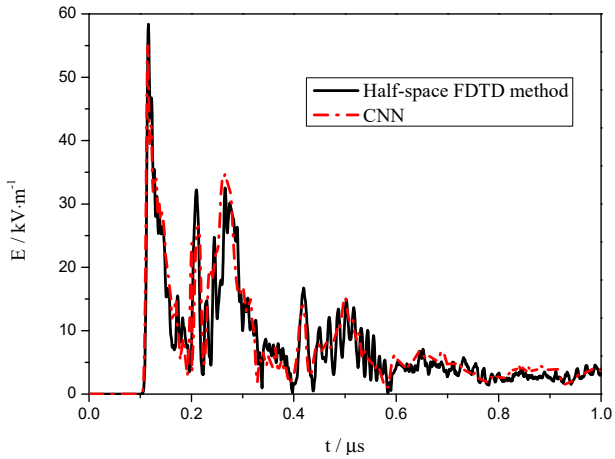

Figure 5. Comparison of electric field predicted by CNN model to half-space FDTD method.

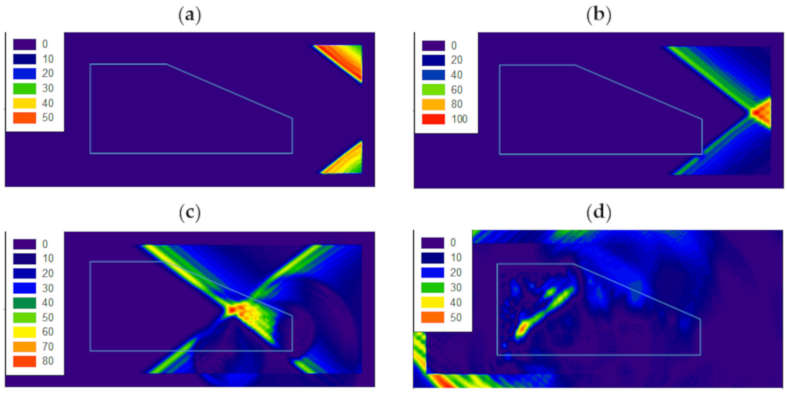

Figure 6. Distribution pattern of the electric field in the *yoz* plane at different time steps. (**a**) Time step = 50; (**b**) time step = 100; (**c**) time step = 200; (**d**) time step = 300.

As shown in Figure 5, the good agreement between the predicted and calculated results indicates the validity and accuracy of the established CNN. In the experiment, the CPU was an Intel (R) Core (TM) i9-10900F CPU @2.80GHz, the GPU was an NVIDIA GeForce RTX 2060, and the training time was about 21 h. When the CNN model is trained, it only takes 1s to complete the prediction, while the traditional half-space method takes 1856 s. At the same time, when the initial conditions are changed, the FDTD method needs to be remodeled and calculated, while the CNN model does not. Therefore, the trained CNN model can significantly improve the analysis efficiency of the HPEMP effect.

3.2. Comparison of Three CNN Models

To compare the performance of three different CNN models, the prediction accuracy and efficiency of LeNet-5, VGG-16, and GoogleNet are shown in Figure 7. The performance testing results of VGG-16 and GoogleNet were acceptable because the two models attained 95% to 98% accuracy and a 0.1–0.4% loss. After 80 iterations, the accuracies of VGG-16 and GoogleNet were maintained at 96%, and the loss was 0.34%. It is evident that the GoogleNet model achieves the highest accuracy and stability in this case, while the accuracy of LeNet-5 is much lower than those of the other two models, and it is unstable and fluctuates significantly. Therefore, this study selected the GoogleNet prediction algorithm. All the experiments in this paper are conducted on an NVIDIA GeForce RTX 2060 GPU, and the CNN framework was an open source in Pytorch. The experiment was performed in the GPU mode.

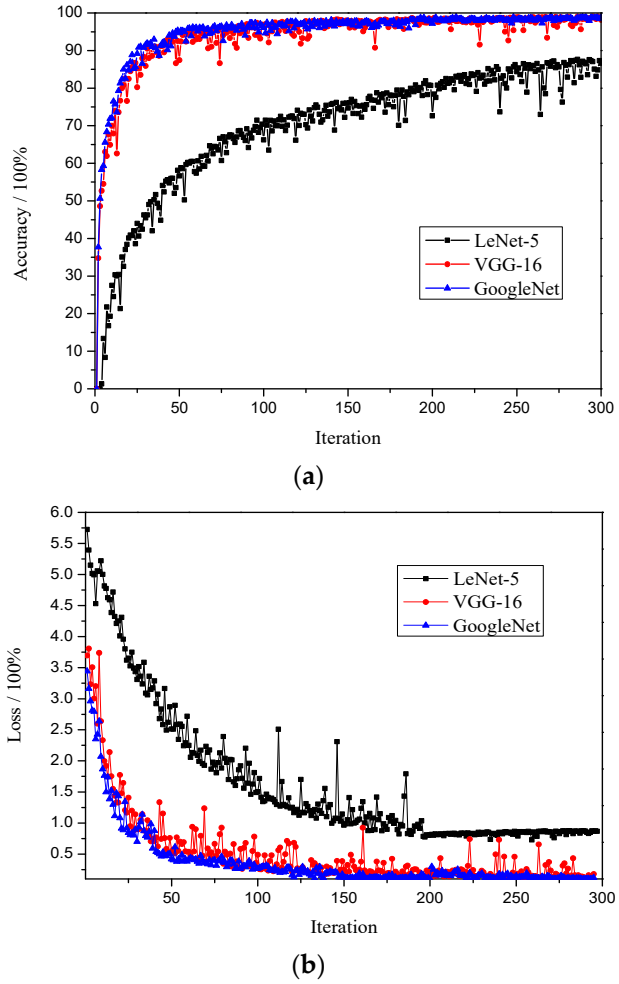

Figure 7. LeNet-5, VGG-16, and GoogleNet models. (**a**) Accuracy; (**b**) loss.

3.3. Discussion

To discuss the prediction results under different half-space medium parameters, three input data were set as A_1 (free space) and A_2 (lossy half-space). The variation in the electric field under HEMP in Equation (3) is shown in Figure 8. It is evident that after a short time delay, the reflected wave arrives at the interior of the vehicle. At the peak and sub-peak of the electric field, the field values increased significantly owing to the effect of the half-space reflected wave. Therefore, the reflected wave of the lower half space cannot be ignored, particularly for strong reflective media, such as a lossy medium. After the direct incident wave brings an energy impact to the sensitive parts inside the ECU, the reflected wave may cause irreversible damage to the sensitive electronic devices.

Since the coupling field is extremely sensitive to the polarization angle α_0, Figure 9 illustrates the comparison of the prediction results under different polarization angles. We set three sets of input data, A_3, A_4, A_5, and A_6, which have the same half-space parameters $\varepsilon_r = 10, \sigma = 0.1S/m$, and the incident wave is the HEMP in Equation (3). It is evident that the field values increase when the polarization angle increases. Consequently, the coupling field from the vertical-polarization ($\alpha_0 = 90°$) case is larger than that from the horizontal-polarization ($\alpha_0 = 0°$) case.

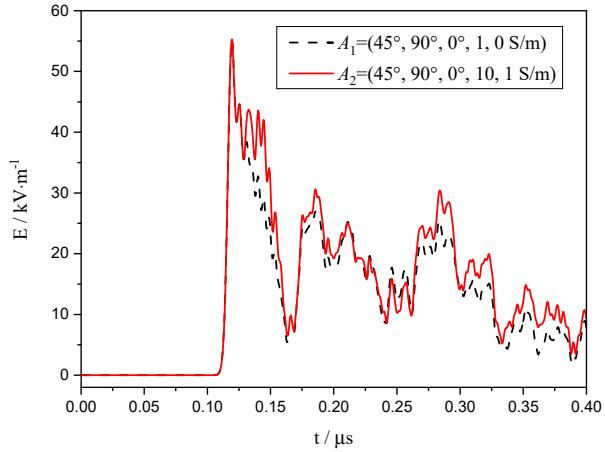

Figure 8. Comparison of coupling electric field in free space and half-space cases.

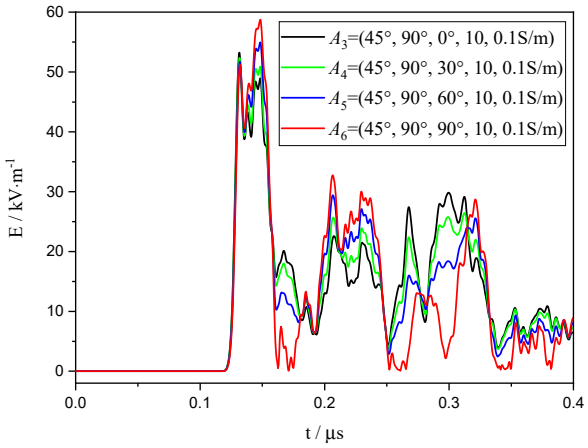

Figure 9. Prediction of electric field with polarization angle.

4. Conclusions

This study proposes a novel prediction method for the HPEMP effect on vehicles using a deep CNN. With the training of a limited number of input datasets, the electric field at the observation point inside the vehicle cab can be analyzed over the half-space. The numerical results demonstrate the feasibility and efficiency of the proposed method. In parallel with traditional numerical algorithms, the proposed method can efficiently predict with low computation cost and memory storage once the CNN network is trained. Furthermore, by comparing the three CNN models, GoogleNet achieved excellent results. Overall, this study makes a preliminary attempt to solve the multiparameter nonlinear HPEMP effect problem based on a combination of numerical methods (not limited to FDTD methods) and deep learning methods. In addition, the proposed method does not need to calculate the half-space Green's function, which can be applied to the complex scattering problem of targets. Consequently, it can provide a reference for the HPEMP effects analysis under different incident conditions and half-space models.

Author Contributions: Conceptualization, L.C. and C.W.; methodology, L.C. and Y.Z.; validation, L.C. and S.H.; writing—original draft preparation, L.C. and S.H.; writing—review and editing, L.C. and Y.Z. All authors have read and agreed to the published version of the manuscript.

Funding: This research was funded in part by the National Natural Science Foundation of China (grant No. 62101433 and 42074225), the China Postdoctoral Science Foundation (grant No. 2019M653634), and the Natural Science Basic Research Plan in Shaanxi Province of China (grant No. 2019JQ-797).

Conflicts of Interest: The authors declare no conflict of interest.

References

1. Backstrom, M.G.; Lovstrand, K.G. Susceptibility of electronic systems to high-power microwaves: Summary of test experience. *IEEE Trans. Electromagn. Compat.* **2004**, *46*, 396–403. [CrossRef]
2. Radasky, W.A.; Baum, C.E.; Wik, M.W. Introduction to the special issue on high-power electromagnetics (HPEM) and intentional electromagnetic interference (IEMI). *IEEE Trans. Electromagn. Compat.* **2004**, *46*, 314–321. [CrossRef]
3. Ängskog, P.; Bäckström, M.; Samuelsson, C.; Kangashaka Vallhagen, B. Shielding effectiveness and HPM vulnerability of energy-saving windows and window Panes. *IEEE Trans. Electromagn. Compat.* **2019**, *61*, 870–877. [CrossRef]
4. Zhang, D.; Zhou, X.; Cheng, E.; Wan, H.; Chen, Y. Investigation on effects of HPM pulse on UAV's datalink. *IEEE Trans. Electromagn. Compat.* **2020**, *62*, 829–839. [CrossRef]
5. Yan, Z.; Qin, F.; Cai, J. Shielding Effectiveness of materials under the excitation of High-Power Microwave. *IEEE Trans. Electromagn. Compat.* **2020**, *62*, 2317–2320. [CrossRef]
6. Cerri, G.; De Leo, R.; Primiani, V.M. Theoretical and experimental evaluation of the electromagnetic radiation from apertures in shielded enclosures. *IEEE Trans. Electromagn. Compat.* **1992**, *34*, 423–432. [CrossRef]
7. Araneo, R.; Lovat, G. Fast MoM analysis of the shielding effectiveness of rectangular enclosures with apertures, metal plates, and conducting objects. *IEEE Trans. Electromagn. Compat.* **2009**, *51*, 274–283. [CrossRef]
8. Liu, Q.F.; Yin, W.Y.; Mao, J.F.; Chen, Z. Accurate characterization of shielding effectiveness of metallic enclosures with thin wires and thin slots. *IEEE Trans. Electromagn. Compat.* **2009**, *51*, 293–300. [CrossRef]
9. Mai, H.; Chen, J.; Zhang, A. A Hybrid algorithm based on FDTD and HIE-FDTD methods for simulating shielding Enclosure. *IEEE Trans. Electromagn. Compat.* **2018**, *60*, 1393–1399. [CrossRef]
10. Liu, Z.; Wang, X. FDTD numerical calculation of shielding effectiveness of electromagnetic shielding fabric based on warp and weft weave points. *IEEE Trans. Electromagn. Compat.* **2020**, *62*, 1693–1702. [CrossRef]
11. Carpes, W.P., Jr.; Pinchon, L.; Razek, A. Analysis of the coupling of an incident wave with a wire inside a cavity using an FEM in frequency and time domains. *IEEE Trans. Electromagn. Compat.* **2002**, *44*, 470–475. [CrossRef]
12. Benhassine, S.; Pinchon, L.; Tabbara, W. An efficient finite-element time-domain method for the analysis of the coupling between wave and shielded enclosure. *IEEE Trans. Magn.* **2002**, *38*, 709–712. [CrossRef]
13. Luo, W.; Liao, Y.; Zhao, Z.G.; Wang, J.; Hu, J.H.; Xie, H.; Zhao, J.Y.; Liu, Q.F.; Zhou, L.; Yin, W.Y. Accurate simulation of shielding effectiveness of metallic cabins using an improved calderon preconditioner-based time-domain integral equation method. *IEEE Trans. Electromagn. Compat.* **2019**, *60*, 200–208. [CrossRef]
14. Cao, L. A new method to calculate induced current of thin wire over anisotropic ground under HPM. *Int. J. Antenn. Propag.* **2019**, *2019*, 4270395. [CrossRef]
15. Hussain, I.; Li, H.; Cao, Q. Multiscale structure simulation using adaptive mesh in DGTD method. *IEEE J. Multiscale Multiphys. Comput. Technnol.* **2017**, *2*, 115–123. [CrossRef]
16. Wei, Y.W.; Wang, C.F.; Kee, C.Y.; Chia, T.T. An accurate model for the efficient simulation of electromagnetic scattering from an object above a rough surface with infinite extent. *IEEE Trans. Antennas Propag.* **2021**, *69*, 1040–1051. [CrossRef]
17. Song, T.; Kuang, L.; Han, L.; Wang, Y.; Liu, Q.H. Inversion of rough surface parameters from SAR images using simulation-trained convolutional neural networks. *IEEE Geosci. Remote Sens. Lett.* **2018**, *15*, 1130–1134. [CrossRef]
18. Li, L.; Wang, L.G.; Teixeira, F.L.; Liu, C.; Nehorai, A.; Cui, T.J. DeepNIS: Deep neural network for nonlinear electromagnetic inverse scattering. *IEEE Trans. Antennas Propag.* **2019**, *67*, 1819–1825. [CrossRef]
19. Cao, L.; Xie, Y.Z.; Gao, M.X. Analysis of time-domain shielding effectiveness of enclosures above lossy half-space using an improved half-space FDTD method. *IEEE Trans. Electromagn. Compat.* **2020**, *62*, 2076–2083. [CrossRef]
20. Chen, S.; Wang, H.; Xu, F.; Jin, Y.Q. Target classification using the deep convolutional networks for SAR images. *IEEE Trans. Geosci. Remote Sens.* **2016**, *54*, 4806–4817. [CrossRef]
21. Kilic, A.; Babaoglu, I.; Babalik, A.; Arslan, A. Through-wall radar classification of human posture using convolutional neural networks. *Int. J. Antenn. Propag.* **2019**, *2019*, 7541814. [CrossRef]
22. Glorot, X.; Antoine, B.; Bengio, Y. Deep sparse rectifier neural networks. In Proceedings of the Fourteenth International Conference on Artificial Intelligence and Statistics, Spokane, WA, USA, 3–8 July 2011; pp. 315–323.
23. Krizhevsky, A.; Sutskever, I.; Hinton, G.E. ImageNet classification with deep convolutional neural networks. In Proceedings of the Advances in Neural Information Processing Systems, Lake Tahoe, NV, USA, 3–6 December 2012; pp. 1097–1105.